



Vol 17, N° 2


<https://revistas.usb.edu.co/index.php/IJPR>

ISSN 2011-2084

E-ISSN 2011-7922

Visual Coding along Multiple Brain Areas

Codificación visual en múltiples áreas del cerebro

Vitória de Araújo Xavier¹ , Nayara da Silva Melo¹ ,
Sidarta Ribeiro² , Nivaldo A P de Vasconcelos^{1,3,4,5*} .

¹ Department of Biomedical Engineering, Federal University of Pernambuco (UFPE), Recife, Pernambuco 50670-901, Brazil.

² Brain Institute, Federal University of Rio Grande do Norte (UFRN), Natal, RN 59056-450, Brazil.

³ Physics Department, Federal University of Pernambuco (UFPE), Recife, Pernambuco 50670-901, Brazil.

⁴ Life and Health Sciences Research Institute (ICVS), School of Medicine, University of Minho, Braga, Portugal.

⁵ ICVS/3B's-PT Government Associate Laboratory, Braga, Portugal.

OPEN ACCESS

Manuscript received: 30-10-2023

Revised: 19-03-2024

Accepted: 26-04-2024

***Corresponding author:**

Nivaldo A P de Vasconcelos

Email: nivaldo.vasconcelos@ufpe.br

Copyright: ©2024. International Journal of Psychological Research provides open access to all its contents under the terms of the license [creative commons Attribution-NonCommercial-NoDerivatives 4.0 International \(CC BY-NC-ND 4.0\)](https://creativecommons.org/licenses/by-nc-nd/4.0/)

Declaration of data availability: All relevant data are within the article, as well as the information support files.

Conflict of interests: The authors have declared that there is no conflict of interest.

How to Cite:

de Araújo Xavier, V., da Silva Melo, N., Ribeiro, S., & de Vasconcelos, N. A. P. (2024). Visual Coding along Multiple Brain Areas. *International Journal of Psychological Research*, 17(2), 54–75. <https://doi.org/10.21500/20112084.7390>



Abstract.

This study focuses on understanding visual coding in multiple brain areas and its implications for neural processing in the visual system. It highlights the use of simultaneous recordings of large neuronal populations to investigate how visual information is encoded and processed in the brain. By studying the activity of multiple brain areas, the paper aims to uncover the mechanisms underlying brain-wide visual perception and provide insights into the neural basis of visual processing. The findings of this research contribute to the broader field of neuroscience and have implications for understanding visual disorders and developing therapeutic interventions.

Resumen.

Este estudio se centra en comprender la codificación visual en múltiples áreas del cerebro y sus implicaciones para el procesamiento neural en el sistema visual. Se destaca el uso de registros simultáneos de grandes poblaciones neuronales para investigar cómo se codifica y procesa la información visual en el cerebro. Al estudiar la actividad de múltiples áreas cerebrales, el artículo tiene como objetivo desvelar los mecanismos subyacentes a la percepción visual a nivel cerebral y proporcionar ideas sobre la base neural del procesamiento visual. Los hallazgos de esta investigación contribuyen al campo más amplio de la neurociencia y tienen implicaciones para entender los trastornos visuales y desarrollar intervenciones terapéuticas.

Keywords.

Sensory Processing, Sensory Coding, Neural Circuits.

Palabras Clave.

Procesamiento sensorial, codificación sensorial, circuitos neuronales.

1. Introduction

Nearly a century ago, Lord Adrian and his colleagues conducted pioneering recordings of sensory and motor neurons, leading them to propose that stimuli properties are encoded by spiking rates (Adrian & Zotterman, 1926; Adrian, 1929). Fueled by Hubel's new Tungsten electrode (Hubel, 1957), in second half of the 1900s, Hubel and Wiesel demonstrated that rate coding in isolated neurons in the primary visual cortex (V1; Hubel & Wiesel, 1959, 1968). Using such technological advancement, they supported an emerging concept in sensory systems termed *receptive field* (Powell & Mountcastle, 1959). Classically, receptive fields are regions of sensory space that elicit a response from a sensory neuron (Hubel & Wiesel, 1962; Powell & Mountcastle, 1959; Ringach, 2004). In vision, a receptive field is the spatial area in which the presence of a light source will modulate the firing rate of that neuron. Since the 1990s, we have a period marked by paramount and sustainable technological developments to provide simultaneously recording large neuronal populations. (Csicsvari et al., 2003; Nicolelis et al., 1997; Nicolelis et al., 2003; Stevenson & Kording, 2011; Steinmetz et al., 2021). Based on such simultaneous recordings of neuronal populations, a novel sensory coding perspective emerged, which expanded the understanding of the nervous. Instead only based on which could be reached from recordings of isolated neurons, that new approach if to study sensory coding is based on patterns observed from neuronal populations, main on their spiking activity (Hung et al., 2005; Vasconcelos et al., 2011).

In recent technological advancements for neural recordings, certain methods leverage silicon-based technologies. These techniques empower us to perform recordings in which a single invasive aperture can accommodate multiple recording sites, arranged with micrometer precision, typically densely packed. This capability leads to what we refer to as "dense recordings". Consequently, these silicon-based technologies have facilitated the simultaneous and dense recording of a unprecedented number of neurons, allowing for the distribution of recording sites across multiple brain areas (Hong & Lieber, 2019; Stevenson & Kording, 2011). Neuropixels are among these silicon-based probes which provide high- count of sites arranged along several millimeters (Durand et al., 2023; Jun et al., 2017; Steinmetz et al., 2018; Steinmetz et al., 2021). Such a great space reach enables us to record multiple areas in 'small' brains. For instance, their recordings usually provide several hundreds of well isolated neurons from multiple brain areas of rodents, mainly from mouse brains.

2. Methods

In Figure 1(a) we provide a comprehensive overview of various recording periods. These include 60 minutes

of exposure to reward-accompanied natural images, 25 minutes to synthetic images (Gabor), 5 minutes to a gray screen (spontaneous), and an additional 60 minutes to natural images without rewards.

Once mice have been adequately trained in the task, they proceed to execute the task while simultaneously recording brain activity through the utilization of Neuropixels probes. This allows for the simultaneous measurement of both neural activity and behavior. Each individual mouse participates in two experimental Neuropixels sessions. In one of these recording sessions, the mice engage in the task using a collection of eight natural scene images that they were exposed to during their training.

This dataset contains recordings that were conducted using Neuropixels 1.0 probes. We performed the insertion of up to 6 probes simultaneously in each mouse over a period of two consecutive recording days. Following the completion of the first recording day, the probes were carefully removed and the mouse was subsequently returned to its designated home cage. Thereby resulting in a total of 300-350 recording sites per probe. Table 1 presents an overview of the sessions studied. For each analyzed session, the sex of the animal, age in days, the number of neuronal units from that session, the recorded and selected areas for the study, as well as the analyzed image group (G or H), are listed.

2.1 Peri-Stimulus Time Histogram

The *PSTH* (Peri-Stimulus Time Histogram) is a graphical representation of a neuron's average firing rate over time, typically in response to a repeated stimulus or set of stimuli. The general mathematical formulation of the *PSTH* involves counting the neuron's spike events in small time intervals and then normalizing by the total stimulus duration or the number of trials. Here is the general mathematical formulation:

Let $R(t)$ be the instantaneous firing rate (or rate density) of the neuron at time t , and $N(t)$ be the number of spikes occurring in the time interval $[t, t+\Delta t]$, where Δt is a small-time interval.

The instantaneous firing rate is calculated as:

$$R(t) = \lim_{\Delta t \rightarrow 0} \frac{N(t)}{\Delta t} \quad (1)$$

The *PSTH* is constructed by summing the number of spikes in discrete time intervals, typically bins, and normalizing by the bin width and the total number of trials:

$$PSTH(t) = \frac{1}{N} \sum_{i=1}^N \frac{1}{\Delta t} \sum_j S_{ij}(t)$$

Where $PSTH(t)$ is the value of the *PSTH* at a specific time interval t , N is the total number of trials or repetitions of the stimulus, $S_{ij}(t)$ is a function that is 1 if a spike occurs in trial i in the time interval t and 0 otherwise and Δt is the bin width in which spikes are counted.

Table 1

Overview of Selected Sessions

ID	Sex	Age	Units	Areas	Group
1055403683	M	144	945	CA1, CA3, DG, LGv, LP, MGd, MGm, MGv, PIL, POL, PoT, SGN, SPFP, TH, VISal, VISam, VISl, VISp, VISpm, VISrl	H
1055415082	F	144	900	CA1, CA3, DG, HPF, LP, MGd, MGm, MGv, PIL, POL, SUB, TH, VISal, VISam, VISl, VISp, VISpm, VISrl	H
1130349290	F	165	1170	CA1, CA3, DG, LGd, LP, MB, MGm, MGv, PoT, SGN, TH, VISal, VISam, VISl, VISp, VISpm, VISrl	G
1120251466	M	131	1497	CA1, CA3, DG, LGd, LP, MGd, MGm, MGv, PIL, ProS, SGN, SUB, VISal, VISam, VISl, VISp, VISpm, VISrl	G
1067781390	M	132	1165	CA1, CA3, DG, HPF, LGd, LP, MB, MGd, MGm, MGv, PIL, POL, PoT, ProS, SGN, SUB, TH, VISal, VISam, VISl, VISp, VISpm, VISrl	H
1063010385	M	134	1049	CA1, CA3, DG, LGd, LP, MB, MGm, MGv, PIL, POL, PoT, PP, SGN, TH, VISal, VISam, VISl, VISp, VISpm, VISrl	H
1044594870	F	152	1201	CA1, CA3, DG, HPF, LP, MB, MGd, MGm, MGv, MRN, PIL, POL, PP, TH, VISal, VISl, VISp, VISpm, VISrl	H
1118512505	F	139	982	CA1, DG, LP, MGd, MGm, MGv, PIL, PoT, ProS, SGN, SUB, TH, VISal, VISam, VISl, VISp, VISpm, VISrl	G
1117148442	M	132	1091	CA1, CA3, DG, HPF, LP, MB, MGd, POL, ProS, SGN, SUB, TH, VISal, VISam, VISl, VISp, VISpm, VISrl	G
1081431006	F	171	1295	CA1, CA3, DG, Eth, HPF, LGd-co, LGd-sh, LP, MGm, MGv, PIL, POL, PoT, PP, ProS, SGN, SNC, SPFP, SUB, TH, VISal, VISam, VISl, VISp, VISpm, VISrl	H

Note. ID refers to the identifier of the analyzed session; Sex to the animal's gender; Age to the days of the animal's life; Neuronal Units to the number of neurons recorded in the session; Areas to the studied brain regions; Group to the batch of images reviewed, marked as G or H. Related Table 2 provides the acronyms used, with their respective full meanings and the macro area to which they belong.

2.2 Gaussian Naive Bayes Classifier

Herein, the Gaussian Naive Bayes classifier was implemented using the model termed GaussianNB from Python scikit-learn. It is based on Bayes' theorem and is commonly used for classification tasks in machine learning. The mathematical formulation for Gaussian Naive Bayes can be described as follows:

Let's assume we have a dataset with N samples, each belonging to one of K classes. We represent the feature vector for each sample as x_i , where i is the sample index, and x_i is a vector of D features: $\mathbf{x}_i = [x_{i1}, x_{i2}, \dots, x_{iD}]$.

In Gaussian Naive Bayes, we make the following assumptions:

- 1. Gaussian Distribution:** The features x_{ij} within each class follow a Gaussian (normal) distribution. In this study x_{ij} is the j -th time bin in the i -th instantaneous firing rate pattern, according to defined in 1;
- 2. Conditional Independence (Naive Assumption):** Features are conditionally independent within each class, meaning that the presence or value of one feature does not affect the presence or value of another feature within the same class. This is a simplifying assumption known as naive Bayes;

The goal is to classify a new data point, \mathbf{x}_{new} , into one of the K classes. Here's the mathematical formulation for Gaussian Naive Bayes:

- 1. Prior Probability:** Calculate the prior probability for each class $P(C_k)$, where k ranges from 1 to K . This represents the probability of each class occurring in the dataset;
- 2. Likelihood:** For each class C_k , calculate the likelihood $P(\mathbf{x}_{\text{new}}|C_k)$, which represents the probability of observing the feature vector \mathbf{x}_{new} given that the class is C_k . This is done using the Gaussian probability density function for each feature:

$$P(\mathbf{x}_{\text{new}}|C_k) = \prod_{j=1}^D \frac{1}{\sqrt{2\pi\sigma_{kj}^2}} \exp\left\{-\frac{(\mathbf{x}_{\text{new},j} - \mu_{kj})^2}{2\sigma_{kj}^2}\right\}$$

where μ_{kj} is the mean of feature j for class C_k , and σ^2 is the variance of feature j for class C_k .

- 3. Posterior Probability:** Use Bayes' theorem to calculate the posterior probability for each class given the new data point:

$$P(C_k|\mathbf{x}_{\text{new}}) = \frac{P(C_k) \cdot P(\mathbf{x}_{\text{new}}|C_k)}{P(\mathbf{x}_{\text{new}})}$$

where $P(C_k)$ is the prior probability for class C_k , $P(\mathbf{x}_{\text{new}}|C_k)$ is the likelihood, and $P(\mathbf{x}_{\text{new}})$ is the evidence or normalization constant.

4. **Classification:** Classify the new data point as belonging to the class with the highest posterior probability:

$$\text{Predict Class} = \text{argmax}P(C_k|\mathbf{x}_{\text{new}})$$

2.3 Pairwise Spiking Correlation

The timescale of spiking synchronization has been proposed in 10–30 ms. However, during the recordings, slow oscillations (frequencies $\ll 30$ Hz) are present in spiking data (Renart et al., 2010). Thus, such recording artifact demands filtering procedure over the spiking data, before the more precise pairwise spiking correlation. Therefore, given a pair of instantaneous firing rate, such as described in Eq. 1, $R_i(t)$ and $R_j(t)$, we calculated the corresponding pairwise spiking correlation, first by convolving each time-series with a proper Mexican-Hat filter, and then we calculated the Pearson correlation over the filtered time-series, zero-mean $\hat{R}_i(t)$ and $\hat{R}_j(t)$, by:

$$r_{i,j} = \frac{\hat{r}_i \cdot \hat{r}_j}{\sigma_i \cdot \sigma_j} \quad (2)$$

where \hat{r}_k is the vector representation of the k -th filtered time-series, $\hat{R}_k(t)$, and σ_k is its corresponding standard-deviation.

3. Results

Herein, receptive fields refer to the visual receptive fields in the mouse visual cortex. These receptive fields are characterized by their selectivity for specific stimulus parameters such as orientation and spatial frequency. The spatial scale of mouse receptive fields is larger compared to other species, but they still exhibit similar selectivity to stimulus parameters (Niell & Stryker, 2008). The current studies have explored more in detail the receptive fields in the primary visual cortex. Section 3.1 shows an initial detailed description of the receptive fields within large neuronal population in the visual cortex, simultaneously recorded, beyond the primary visual cortex.

The peristimulus time histogram (*PSTH*) is a valuable tool for analyzing the consistency of spiking responses of neuronal populations for a given event. In the current study, the events were visual stimuli from different classes: natural images and synthetic images (Gabor), both with a duration of 2.5 s, 100 samples/session/class, randomly selected. The primary novelty of this study was the simultaneous observation of spiking responses of neuronal populations across multiple brain areas under well-defined visual stimuli. In section 3.2, we evaluated brain areas and categorized them into three main regions: visual cortex, thalamus, and hippocampus,

details of which are provided in Table 2. This table includes the primary area, the corresponding subregions for each area, their specific acronyms, and the number of neurons recorded in each subarea. It is important to note that, in total, the recordings encompassed 11295 neurons.

3.1 Receptive Fields along the Visual Cortex

In Figure 1 we present an exploration of spiking activity along the visual cortex (VIS). The visual cortex is divided into distinct regions: VISp (primary visual cortex), VISpm (posteromedial), VISl (lateromedial), VISrl (rostrolateral), VISal (anterolateral), and VISam (anteromedial). In Figure 1(b) we showcase samples of 945 identified receptive fields across the visual cortex, representing a subset of 4650 recorded units in the group data (10 sessions). The distribution of identified receptive fields is as follows: #VISal=177, #VISam=110, #VISl=257, #VISp=173, #VISpm=143, and #VISrl=85. In (c), we analyze spiking correlation structures along the visual cortex. Notably, we report average correlation values (Eq. 2) for different regions: VISal = .0167, VISam = .0052, VISl = .0164, VISp = .0164, VISpm = .0071, and VISrl = .0114. These correlation values provide insights into the functional relationships between different regions of the visual cortex. The figure provides a comprehensive view of spiking activity and correlation structures within the visual cortex, shedding light on its response patterns under spontaneous activity along the mouse visual cortex in head-fixed recordings.

3.2 Spiking Response for Different Visual Stimuli along Brain Areas

Visual cortex. Figure 2 shows the population group data *PSTH* (peristimulus time histogram) in different regions of the (VIS p = primary visual cortex, pm = posteromedial, l = lateromedial, rl = rostrolateral, al = anterolateral, am = antero-medial) under different visual stimuli. The number of sessions n is indicated in each plot. The vertical axis represents the mean instantaneous firing rate of the population (spikes/neurons/second). The results showed that *PSTH* responses to natural stimuli were stronger and more sustained than the *PSTH* responses to synthetic stimuli in all regions of the visual cortex. This suggests that neurons in the visual cortex are more responsive to natural stimuli than to synthetic stimuli. Additionally, the *PSTH* responses to natural stimuli showed a greater degree of variability across different regions of the visual cortex than the *PSTH* responses to synthetic stimuli. This suggests that different regions of the visual cortex are differentially involved in processing natural stimuli. The primary visual area has the ability to discriminate spatial details, such as orientation (Marshall et al., 2011; Prusky & Douglas, 2004). The lateromedial area (lm) is more specialized in processing fast movements, as its neurons

Table 2

Detailed Information from Selected Recorded Areas

Area	Subarea	Acronym	Neurons
Visual Cortex	primary visual cortex	VISp	897
	posteromedial area	VISpm	806
	anterolateral area	VISal	748
	lateromedial area	VISl	915
	rostrolateral area	VISrl	537
	anteromedial area	VISam	747
	Total		4650
Hippocampus	cornu ammonis 1	CA1	2110
	cornu ammonis 3	CA3	586
	dentate gyrus	DG	852
	subiculum	SUB	397
	hippocampal formation	HPF	112
	prosubiculum	ProS	69
	Total		4136
Thalamus	posterior lateral thalamic nucleus	LP	322
	ventral medial geniculate complex	MGv	584
	medial medial geniculate complex	MGm	175
	dorsal medial geniculate complex	MGd	219
	posterior intralaminar thalamic nucleus	PIL	114
	supragenulate nucleus	SGN	284
	thalamus	TH	146
	posterior limitans thalamic nucleus	POL	226
	posterior triangular thalamic nucleus	PoT	128
	lateral geniculate complex dorsal part	LGd	200
	lateral geniculate complex ventral part	LGv	24
	peripeduncular nucleus	PP	44
	ethmoid thalamic nucleus	Eth	37
	subparafascicular nucleus	SPFp	6
	Total		2509
	Total		11295

have a higher preference for elevated temporal frequencies, a characteristic shared with the anteromedial region (am). The anterolateral (al) region of the visual cortex is functionally distinct from other areas and is specialized for motion-related computations (Marshel et al., 2011). This area, along with the rostrolateral (rl) and anteromedial (am) regions, contains neurons highly selective for the direction of movement and integrates the parietal cortex, associated with spatial discrimination and navigation tasks (Kravitz et al., 2011; Marshel et al., 2011; Ungerleider and Mishkin, 1982; Whitlock et al., 2008).

The posteromedial area mediates visual information between primary visual cortex and the retrosplenial cortex in rodents (Marshel et al., 2011; Roth et al., 2012; Wang & Burkhalter, 2007). The highest average instantaneous firing rate for natural stimuli was observed in the primary region (p), followed by the lateromedial (l) and anterolateral (al) regions. The rostrolateral region (rl) comes next, and, finally, the posteromedial (pm) and anteromedial (am) regions. On the other hand, the highest average instantaneous firing rate for synthetic stimuli was observed in the anterolateral region (al), followed by the

lateromedial (lm), rostromedial (rl), anteromedial (am), primary (p), and posteromedial (pm) areas. This suggests that the primary region of the visual cortex is more involved in processing natural stimuli than the anterior region of the visual cortex.

Table 3 shows that, in general terms, significant differences were identified between the PSTHs of the regions recorded in the visual cortex for natural stimuli ($p < .01$, Mann-Whitney), except between the lateromedial regions (VISl) and posteromedial (VISpm) ($p = .2177$, Mann-Whitney). This suggests that the distributions of response amplitudes in average population activity do not vary significantly throughout the visual cortex.

Table 3

P-values Obtained from the Mann-Whitney Test from Different Regions of the Visual Cortex

	VISal	VISam	VISrl	VISl	VISp	VISpm
VISal	–	.0	.0	.0	.0	.0
VISam	–	–	.0	.0	.0	.0
VISrl	–	–	–	.0	.0	.0
VISl	–	–	–	–	.0	.2177
VISp	–	–	–	–	–	.0003
VISpm	–	–	–	–	–	–

Note. The values were used to compare the PSTH values derived from different regions of the visual cortex (VIS al = anterolateral, am = anteromedial, rl = rostromedial, l = lateromedial, p = primary visual cortex, pm = posteromedial) for natural stimuli.

Hippocampus. Based on the results on from visual spiking activity, we decided to explore the consistency of the spiking response pattern for visual stimuli along hippocampus areas (HPF, CA1, CA3, DG, SUB, ProS), such as detailed in Figure 3. The number of sessions ($n = 10, 9, 6, 5$, respectively) is indicated on each plot. The results show that the PSTH responses to natural stimuli are stronger and more sustained than the PSTH responses to synthetic stimuli in most regions of the hippocampus. This suggests that neurons in the hippocampus are more responsive to natural stimuli than to synthetic stimuli. However, the difference in PSTH responses between natural and synthetic stimuli is less pronounced in the SUB region of the hippocampus. The hippocampal formation (HPF), composed of the hippocampus HP, dentate gyrus (DG), and subiculum (SUB), is crucial for the creation of episodic memories, albeit not being their ultimate storage location (Kandel, 2013). The hippocampus is pivotal for long-term memories, partakes in object recognition, episodic memory, and is indispensable for spatial representation and navigation (Andersen et al., 2007; Kandel, 2013). The CA1 area is vital for the consolidation and retrieval of long-term explicit memory, while the CA3 area manages the initial encoding and storage of information, also playing a role in memory formation and retrieval through pattern completion and

separation (Kandel, 2013). The DG in the hippocampus is essential in the creation of new memories and in distinguishing between similar memories or experiences (Kandel, 2013). The SUB, a part of the subicular complex, processes information about space, movement, and memory, and regulates stress response (O'Mara, 2005). Finally, the ProS is the transition zone between the CA fields and the SUB, being relevant for the memory system of the medial temporal lobe and connected to neurological conditions such as Alzheimer's and epilepsy, also being associated with emotion, motivation, reward, drug dependence, stress, anxiety, and fear (Amaral et al., 1990; Ding, 2013). The highest average instantaneous firing rate for natural stimuli is found in the ProS region of the hippocampus, while the highest average instantaneous firing rate for synthetic stimuli is found in the CA1 region of the hippocampus. This suggests that the ProS region of the hippocampus is more involved in the processing of natural stimuli, whereas that CA1 region is more involved in the processing of synthetic stimuli. In summary, the findings depicted in Figure 3 indicate that hippocampal neuronal populations exhibit a higher degree of responsiveness to natural stimuli in comparison to synthetic ones. Moreover, the spiking response patterns to visual stimuli exhibit a diverse level of consistency throughout the areas of the hippocampal formation. Table 4 shows that, in general terms, significant differences were identified between the PSTHs of the regions recorded in the hippocampus for natural stimuli ($p < .01$, Mann-Whitney), except between the hippocampal formation (HPF) and prosubiculum ProS ($p = .00350$, Mann-Whitney). This suggests that the distributions of response amplitudes in average population activity do not vary significantly throughout the hippocampus.

Table 4

P-values Obtained from the Mann-Whitney Test from Different Regions of the Hippocampus

	HPF	CA1	CA3	DG	SUB	ProS
HPF	–	.0	.0	.0	.0	.0
CA1	–	–	.0	.0	.0	.0
CA3	–	–	–	.0	.0	.0
DG	–	–	–	–	.0	.0
SUB	–	–	–	–	–	.0
ProS	–	–	–	–	–	–

Note. Values were used to compare the PSTH values derived from different regions of the hippocampus (HPF, CA1, CA3, DG, SUB, ProS) for natural stimuli.

Thalamus. Figures 4 and 5 present the population PSTH (Peri-stimulus Time Histogram) group data across different Thalamic (TH) regions: (TH, LGd, LGv, MGd, MGvm, MGv, LP, SGN, PIL, POL, PoT, PP, Eth, SPFp) under varying visual stimuli. The session number n is depicted in each graph. The results demonstrated stronger and more sustained PSTH responses to natu-

Table 5

The *p*-values obtained from the Mann-Whitney test from Different Regions of the Thalamus

	TH	LGd	LGv	MGd	MGm	MGv	LP	SGN	PIL	POL	Pot	PP	Eth	SPFp
TH	–	.0	.0	.0	.0	.0	.0	.0023	.0	.0	.0	.0	.0	.0
LGd	–	–	.0	.0	.0	.0	.0	.0	.0	.0	.0	.0	.0	.0
LGv	–	–	–	.0	.0	.0	.0	.0	.0	.0	.0	.0	.0	.0
MGd	–	–	–	–	.0	.0	.0	.0	.0	.0	.0	.0	.0	.0
MGm	–	–	–	–	–	.0	.0	.0	.0	.0	.0	.0	.0	.0
MGv	–	–	–	–	–	–	.0	.0	.0	.0	.0316	.0	.0	.0
LP	–	–	–	–	–	–	–	.0	.0	.0	.0	.0	.0	.0
SGN	–	–	–	–	–	–	–	–	.0	.0	.0	.0	.0	.0
PIL	–	–	–	–	–	–	–	–	–	.0	.0	.0	.0	.0
POL	–	–	–	–	–	–	–	–	–	–	.0	.0	.0	.0
PoT	–	–	–	–	–	–	–	–	–	–	–	.0	.0	.0
PP	–	–	–	–	–	–	–	–	–	–	–	–	.0	.0
Eth	–	–	–	–	–	–	–	–	–	–	–	–	–	.0
SPFp	–	–	–	–	–	–	–	–	–	–	–	–	–	–

Note. Values were used to compare the *PSTH* values derived from different regions of the hippocampus (HPF, CA1, CA3, DG, SUB, ProS) for natural stimuli.

ral stimuli compared to synthetic ones in most thalamic regions, indicating a higher responsiveness of thalamic neurons to natural stimuli. The Lateral Posterior Thalamic Nucleus (LP), which seems to be associated with determining visual saliency and visually guided behaviors, is involved in multisensory processing of aversive stimuli-related information alongside the dorsal portions of the Posterior Thalamic Nuclei (Po) (Allen et al., 2016). The Medial Geniculate Complex, encompassing ventral (MGv), dorsal (MGd), and medial (MGm) subnuclei, predominantly relates to auditory functions, conveying information from the midbrain to the auditory cortex (LeDoux et al., 1984; Watson et al., 2011). The Posterior Intralaminar Thalamic Nucleus (PIL) is associated with the regulation of information transmission such as cognition, alertness, consciousness, and pain signal processing (Arnts et al., 2023). The Suprageniculate Nucleus (SGN) contributes to the amalgamation of visual, auditory, and somatosensory information, especially nociceptive, from varied sources, projecting them to the amygdala (Watson et al., 2011). It might also be associated with generating visual information for the auditory cortex (Smith et al., 2010). The Posterior Limitans Thalamic Nucleus (POL) is implicated in the processing of visual and somatosensory information and aversive stimuli (Paxinos & Franklin, 2001; Watson et al., 2011). The Posterior Triangular Thalamic Nucleus (PoT) is primarily linked to the perception of pain sensations (Gauriau & Bernard, 2004). The Lateral Geniculate Complex, both dorsal (LGd) and ventral (LGv) parts, belongs to the category of thalamus sensory projection nuclei and is essential for normal visual processing. It has extensive connectivity, projecting to and receiving inputs (Covington & Al Khalili, 2019). The Peripeduncular Nucleus (PP) is associated with motor performance (Zrinzo et al., 2007). The Subparafasci-

cular Nucleus Parvicellular Part (SPFp) has a medial part implicated in the relay of genitosensory information crucial for male sexual behavior, while its lateral part is engaged in processing auditory and visual signals related to fear-conditioned responses (Coolen et al., 2003). The Ethmoid Thalamic Nucleus (Eth) refers to a group of centrally located cells in the posterior portion of the mouse thalamus (Paxinos & Franklin, 2001; Watson et al., 2011). The highest average instantaneous firing rate for natural stimuli was observed in the SPFp region, followed by the PP region. These regions also demonstrated the highest firing rates for synthetic stimuli, suggesting their significant involvement in processing both stimuli types. Subsequently, the LP region has a high average instantaneous firing rate for natural stimuli compared to synthetic, indicating its greater involvement in processing natural stimuli. Table ?? shows that, generally, significant differences were observed between the *PSTHs* of the regions recorded in the thalamus for natural stimuli ($p < .01$, Mann-Whitney), except between the ventral medial geniculate complex (MGv) and the posterior triangular thalamic nucleus (PoT; $p = .0316$, Mann-Whitney). This suggests that the distributions of response amplitudes in average population activity do significantly vary throughout the thalamus.

3.3 Spiking Patterns Classification for Different Kinds of Visual Stimuli along Brain Areas

Given the striking differences observed among the peristimulus time histograms (*PSTHs*) elicited by natural and synthetic stimuli, we decided to assess the separability of spiking patterns in response to these distinct stimulus types. This estimation involved a binary classifier model: Naive Bayes. This model was provided with firing rate patterns from their respective neuronal populations, each consisting of a 250 ms duration and

sampled at 1 ms intervals, and was appropriately labeled (Hung et al., 2005; Vasconcelos et al., 2011). The evaluation of classification performance was based on the average area under the Receiver Operating Characteristic (ROC) curve across 20 trials (Fawcett, 2006), conducted for each specific data context (session/area).

Visual Cortex. The first graph in Figure 6 displays a boxplot that depicts the average area under the ROC curve (AUROC) for Naïve Bayes classification of natural versus synthetic visual stimuli across various regions of the visual cortex, identified as anterolateral (al), anteromedial (am), rostrolateral (rl), lateromedial (l), primary visual cortex (p), and posteromedial (pm). The dotted gray line in the graphs signifies the chosen AUROC threshold considered as indicative of high-quality classification ($> .75$). All visual cortex areas were observed to exceed this threshold, reflecting the Naïve Bayes method's effectiveness in classifying stimuli by their origin. These findings support and broaden previous research on the encoding of visual stimuli within the mammalian visual cortex. The results indicate that the AUROC for natural stimuli is consistently higher than for synthetic across all studied regions, suggesting a higher accuracy of Naïve Bayes in distinguishing natural from synthetic stimuli as compared to different types of synthetic stimuli. As shown in Table 6, statistically significant differences were noted in the AUROC averages for natural stimuli among the recorded regions ($p < .01$, Mann-Whitney test), with the exception of comparisons between the al and rl regions ($p = .1206$, Mann-Whitney test) and between am and al ($p = .0989$, Mann-Whitney test).

Table 6

P-values Obtained from the Mann-Whitney Test from Classifications using the Naïve Bayes Classifier across Different Regions of the Visual cortex

	VISal	VISam	VISrl	VISl	VISp	VISpm
VISal	–	.0	.0	.0047	.1206	.0
VISam	–	–	.0989	.0	.0	.0
VISrl	–	–	–	.0	.0	.0
VISl	–	–	–	–	.0	.0
VISp	–	–	–	–	–	.0054
VISpm	–	–	–	–	–	–

Note. Values were used to compare the AUC values derived from classifications using the Naïve Bayes classifier across different regions of the visual cortex (VIS al = anterolateral, am = anteromedial, rl = rostrolateral, l = lateromedial, p = primary visual cortex, pm = posteromedial).

Hippocampus. In assessing the discrimination ability between two categories of visual stimuli applied to the hippocampus, our findings indicate that the HPF, CA1, and SUB regions demonstrate high classification quality (AUROC $> .75$). This is illustrated in the central boxplot in Figure 6, which displays the average area

under the ROC curve for Naïve Bayes classification between natural and synthetic visual stimuli in different regions of the hippocampus: (HPF, CA1, CA3, DG, SUB, ProS). The lowest AUROC average is observed in the ProS region (AUROC $< .7$), with intermediate results for the CA3 and DG regions. From the standpoint of sensory information processing, particularly visual stimuli, hippocampal neurons are most renowned for encoding location, with their place cells (O'Keefe, 1976). Just as Bourboulou et al. discovered that the introduction of local visual cues enhances the resolution of spatial encoding in the hippocampus, resulting in reduced local fields and heightened spatial selectivity (Bourboulou et al., 2019), our current results expand the understanding of visual stimuli encoding in different areas of the hippocampus. Table 7 reveals significant differences between the AUROC averages of the regions recorded in the hippocampus for natural stimuli ($p < .01$, Mann-Whitney), except between HPF and CA1 ($p = .8805$, Mann-Whitney), between HPF and SUB ($p = .0502$, Mann-Whitney), and between CA3 and DG ($p = .8807$, Mann-Whitney).

Table 7

P-values Obtained from the Mann-Whitney Test from lClassifications using the Naïve Bayes Classifier

	HPF	CA1	CA3	DG	SUB	ProS
HPF	–	.8805	.0003	.0005	.0502	.0
CA1	–	–	.0	.0	.0047	.0
CA3	–	–	–	.8807	.0	.0
DG	–	–	–	–	.0	.0
SUB	–	–	–	–	–	.0
ProS	–	–	–	–	–	–

Note. Values were used to compare the AUC values derived from classifications using the Naïve Bayes classifier across different regions of the hippocampus (HPF, CA1, CA3, DG, SUB, ProS).

Thalamus. The last boxplot shown in Figure 6 presents the average area under the ROC curve for the thalamic areas: (TH, LGd, LGv, MGd, MGvm, MGv, LP, SGN, PIL, POL, PoT, PP, Eth, SPFp). The results generally demonstrate high classification quality (AUROC $> .75$) for the areas: TH, LGd, LGv, MGv, LP, SGN, PP, and Eth. For the areas PIL, POL, and PoT, there were intermediate results with average AUROC between .7 and .75. However, for the regions: MGd, MGvm, and SPFp, the results did not demonstrate good performance. These results show that it is possible to distinguish between natural and synthetic visual stimuli and encourage understanding about the encoding of visual stimuli in different areas of the thalamus. Table 8 reveals significant differences between the average AUROCs of the regions recorded in the thalamus for natural stimuli ($p < .01$, Mann-Whitney), except between TH

Table 8

The *p*-values Obtained from the Mann-Whitney Test from Classifications using the Naïve Bayes Classifier across Different Regions of the Thalamus

	TH	LGd	LGv	MGd	MGm	MGv	LP	SGN	PIL	POL	Pot	PP	Eth	SPFp
TH	–	.0	.0	.0	.0	.0	.0	.0023	.0	.0	.0	.0	.0	.0
LGd	–	–	.0	.0	.0	.0	.0	.0	.0	.0	.0	.0	.0	.0
LGv	–	–	–	.0	.0	.0	.0	.0	.0	.0	.0	.0	.0	.0
MGd	–	–	–	–	.0	.0	.0	.0	.0	.0	.0	.0	.0	.0
MGm	–	–	–	–	–	.0	.0	.0	.0	.0	.0	.0	.0	.0
MGv	–	–	–	–	–	–	.0	.0	.0	.0	.0316	.0	.0	.0
LP	–	–	–	–	–	–	–	.0	.0	.0	.0	.0	.0	.0
SGN	–	–	–	–	–	–	–	–	.0	.0	.0	.0	.0	.0
PIL	–	–	–	–	–	–	–	–	–	.0	.0	.0	.0	.0
POL	–	–	–	–	–	–	–	–	–	–	.0	.0	.0	.0
PoT	–	–	–	–	–	–	–	–	–	–	–	.0	.0	.0
PP	–	–	–	–	–	–	–	–	–	–	–	–	.0	.0
Eth	–	–	–	–	–	–	–	–	–	–	–	–	–	.0
SPFp	–	–	–	–	–	–	–	–	–	–	–	–	–	–

Note. Values were used to compare the AUC values derived from classifications using the Naïve Bayes classifier across different regions of the thalamus (TH, LGd, LGv, MGd, MGm, MGv, LP, SGN, PIL, POL, PoT, PP, Eth, SPFp).

and LP ($p = .0544$, Mann-Whitney), TH and SGN ($p = .6432$, Mann-Whitney), TH and Eth ($p = .9756$, Mann-Whitney), MGm and POL ($p = .1202$, Mann-Whitney), MGm and PoT ($p = .15$, Mann-Whitney), MGv and LP ($p = .8432$, Mann-Whitney), MGv and PP ($p = .2052$, Mann-Whitney), LP and SGN ($p = .5331$ Mann-Whitney), LP and Eth ($p = .2406$, Mann-Whitney), SGN and Eth ($p = .7005$, Mann-Whitney), PIL and POL ($p = .0548$, Mann-Whitney), PIL and PoT ($p = .0833$, Mann-Whitney), PIL and Eth ($p = .0267$, Mann-Whitney), POL and PoT ($p = .5654$, Mann-Whitney), and PoT and Eth ($p = .1125$, Mann-Whitney).

3.4 Distributed Encoding of Visual Stimulus across the Recorded Regions

Given the relevant results in evaluating the separability of firing patterns in response to these different types of stimuli, we sought to assess the decoding capability of the stimulus identity based solely on spike recordings for an increasing number of neurons randomly chosen, ranging from 2 to 40. This estimation involved the Naive Bayes classifier, with 10-fold cross-validation, fed with firing rate patterns from their respective neuronal populations, with random samples of 250 samples from the population, each with a duration of 250 ms and sampled at 1 ms intervals. The evaluation of the classification performance was based on the average area under the Receiver Operating Characteristic (ROC) curve over 20 attempts for each amount of neurons (Fawcett, 2006), conducted for each specific data context (session/area).

Visual Cortex. Figure 7 presents the results of neuron dropping in several regions of the visual cortex, labeled as VIS: al = anterolateral, am = anteromedial, rl = rostrolateral, l = lateromedial, p = primary visual cortex, pm=posteromedial.

It depicts the relationship between the average ROC curve from the 20 trials on the *y*-axis and the respective value of evaluated neurons on the *x*-axis. The curves indicate the commencement of a stabilization process of the average AUROC at around 20 to 30 neurons across all regions of the visual cortex. This observation implies that identifying the visual stimulus is plausible with a minimal neuron set, containing specific information pertinent to the stimulus.

Hippocampus. For the hippocampal region, the results are presented in Figure 8 with the regions HPF, CA1, CA3, DG, SUB, ProS. In it, the relationship between the average ROC curve on the *y*-axis of the 20 trials, and on the *x*-axis the respective value of evaluated neurons is displayed. The curves show that the classification processes begin a stabilization process of the average AUROC for most of the hippocampal regions at approximately 20 to 35 neurons. This suggests that the identification of the visual stimulus is possible with a reduced set of neurons; these results validate and expand the perspective of visual stimulus encoding in hippocampal regions, even when analyzing a small set of neurons.

Thalamus. Finally, for the different regions of the thalamus: TH, LGd, LGv, MGd, MGm, MGv, LP, SGN, PIL, POL, PoT, PP, Eth, SPFp, Figures 9 and 10 display the relationship between the average of the ROC curve on the *y*-axis of the 20 trials, and on the *x*-axis the respective value of evaluated neurons. The curves show that the classification processes begin a stabilization process of the average AUROC for most of the thalamic regions from a random set of approximately 10 neurons, up to regions that gain this stability later, at approximately 30 neurons, such as MGv, SGN, and Eth. Even so, the results present the possibility of decoding with

a small set of neurons (< 40) for the thalamic regions, expanding the perspective of encoding visual stimuli in these regions.

4. Discussion

Understanding how the brain processes visual information can have implications for the development of advanced artificial intelligence systems that can mimic mammal's visual perception and recognition, including human visual perception. The findings of this study can contribute to the development of more effective treatments for visual disorders and impairments by providing insights into the neural mechanisms involved in visual coding. The simultaneous recording of brain wide large neuronal populations of mammals, as explored in this paper, can pave the way for the development of more accurate brain-computer interfaces, allowing individuals with motor disabilities to control external devices using their brain activity. The research on visual coding in multiple brain areas can also have implications for the field of neuroscience, helping to deepen our understanding of how different brain regions interact and collaborate in processing visual information.

High-density silicon electrodes have begun to transform systems neuroscience (Trautmann et al., 2023). Until 2010, it was hegemonic a view of a cortical processing based on highly correlated spiking activity (Cohen & Kohn, 2011). However, more recently, has been demonstrated that the spiking activity in the visual cortex, mainly the primary visual cortex, displays a rich and diverse dynamics (Fontenele et al., 2019), including an asynchronous spiking activity (Renart et al., 2010; Ecker et al., 2010). Here, showed an asynchronous spiking activity under spontaneous activity based on simultaneous recordings along the visual cortex, with a tendency for smaller average spiking correlation in its posteromedial and anteromedial areas.

Based on high-density and brain-wide recordings from neuropixels (Jun et al., 2017; Steinmetz et al., 2021), it was possible to investigate, simultaneously, the visual coding beyond the visual cortex, including in areas poorly explored regarding the such subject. Using machine learning techniques, we have consolidated the concept that the encoding of relevant functions of the nervous system is not a localized phenomenon, but rather a comprehensive process within the brain (Lashley, 1930; Nicolelis & Lebedev, 2009; Vasconcelos et al., 2011). This principle is evidenced when we observe visual encoding not only in the visual cortex but also in regions such as the hippocampus and thalamus. The results reinforce this view by demonstrating the feasibility of differentiating between natural and synthetic stimuli using classifiers, indicating that the encoding of stimuli extends beyond the areas traditionally associated with vision, suggesting a more widespread and integrated dis-

tribution of neural activity related to visual perception throughout the brain. According to Figure 6, among these areas, only small minority of thalamic and hippocampal regions did not display good information to classify the kind of visual stimuli. Further, even with a diverse quality classification along brain areas, the distribution of information used in visual coding seems to be equally distributed when observed local sub-regions of visual cortex, hippocampus and thalamus. Therefore, based on evidence obtained from comprehensive, high-density recordings spanning the entire brain, this study suggests that Lashley's theories on information processing in the nervous system be reconsidered. As for the future work, it suggests investigating the decoding capacity in other brain regions such as the midbrain and using various natural visual stimuli to explore these questions further. However, one limitation of this study is the high computational cost associated with analyzing these data sets. The extensive resources required necessitate the use of supercomputing to process the results in a timely manner.

5. Acknowledgements

N.A.P.V. was a recipient of CNPq Grant 249991/2013-6 and CAPES Grant 88887.131435/2016-00. This work was developed under the scope of the project NORTE-01-0145-FEDER-000013, supported by the Northern Portugal Regional Operational Programme (NORTE 2020), under the Portugal 2020 Partnership Agreement, through the European Regional Development Fund (FEDER). This research was supported by NPAD/UFRN. NAPV thanks IL de Vasconcelos for reviewing or editing the manuscript.

References

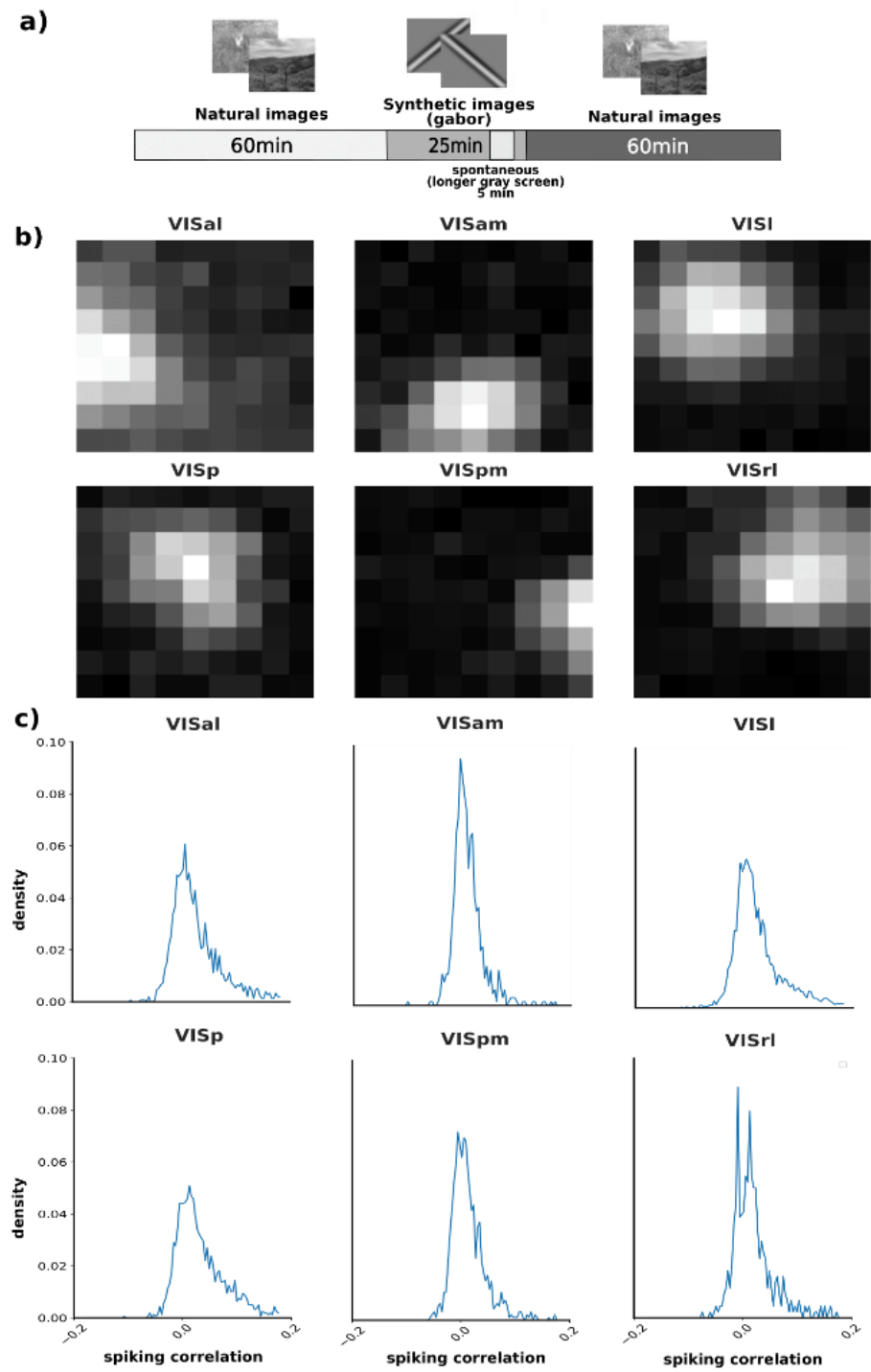
- Adrian, E. (1929). "Motor nerve fibers. Part ii. The frequency of discharge in reflex and voluntary contractions". *J. Physiol.*, *67*, 119–151.
- Adrian, E. D., & Zotterman, Y. (1926). The impulses produced by sensory nerve endings: Part 3. Impulses set up by touch and pressure. *J. Physiol.*, *61*(4), 465–483.
- Allen, A. E., Procyk, C. A., Howarth, M., Walmsley, L., & Brown, T. M. (2016). Visual input to the mouse lateral posterior and posterior thalamic nuclei: Photoreceptive origins and retinotopic order. *The Journal of Physiology*, *594*(7), 1911–1929.
- Amaral, D., Insausti, R., & Paxinos, G. (1990). The human nervous system. *San Diego: Academic*, 711–755.
- Andersen, P., Morris, R., Amaral, D., Bliss, T., & O'Keefe, J. (2007). *The hippocampal formation*. Oxford University Press.

- Arnts, H., Coolen, S. E., Fernandes, F. W., Schuurman, R., Krauss, J. K., Groe-newegen, H. J., & van den Munckhof, P. (2023). The intralaminar thalamus: a review of its role as a target in functional neurosurgery. *Brain Commun*, *5*(3), fcad003.
- Bourboulou, R., Marti, G., Michon, F.-X., El Feghaly, E., Nouguiet, M., Robbe, D., Koenig, J., & Epstein, J. (2019). Dynamic control of hippocampal spatial coding resolution by local visual cues. *Elife*, *8*, 44487.
- Cohen, M. R., & Kohn, A. (2011). Measuring and interpreting neuronal correlations. *Nature Neuroscience*, *14*(7), 811–819.
- Coolen, L. M., Veening, J. G., Wells, A. B., & Shipley, M. T. (2003). Afferent connections of the parvocellular subparafascicular thalamic nucleus in the rat: evidence for functional subdivisions. *Journal of Comparative Neurology*, *463*(2), 132–156.
- Covington, B. P., & Al Khalili, Y. (2019). *Neuroanatomy, nucleus lateral geniculate*. StatPearls Publishing.
- Csicsvari, J., Henze, D. A., Jamieson, B., Harris, K. D., Sirota, A., Barthó, P., Wise, K. D., & Buzsáki, G. (2003). Massively parallel recording of unit and local field potentials with silicon-based electrodes. *J. Neurophysiol*, *90*(2), 1314–1323. <https://doi.org/10.1152/jn.00116.2003>
- Ding, S.-L. (2013). Comparative anatomy of the prosubiculum, subiculum, presubiculum, postsubiculum, and parasubiculum in human, monkey, and rodent. *Journal of Comparative Neurology*, *521*(18), 4145–4162.
- Durand, S., Heller, G. R., Ramirez, T. K., Luviano, J. A., Williford, A., Sullivan, D. T., Cahoon, A. J., Farrell, C., Groblewski, P. A., Bennett, C., Siegle, J. H., & Olsen, S. R. (2023). Acute head-fixed recordings in awake mice with multiple neuropixels probes. *Nature Protocols*, *18*(2), 424–457. <https://doi.org/10.1038/s41596-022-00768-6>
- Ecker, A. S., Berens, P., Keliris, G. A., Bethge, M., Logothetis, N. K., & Tolias, A. S. (2010). Decorrelated neuronal firing in cortical microcircuits. *Science*, *327*(5965), 584–587.
- Fawcett, T. (2006). An introduction to roc analysis. *Pattern recognition letters*, *27*(8), 861–874.
- Fontenele, A. J., Vasconcelos, N. A. P., Feliciano, T., Aguiar, L. A. A., Soares- Cunha, C., Coimbra, B., Dalla Porta, L., Ribeiro, S., Rodrigues, A. J., Sousa, N., Carelli, P. V., & Copelli, M. (2019). Criticality between cortical states. *Physical Review Letters*, *122*(20), 208101. <https://doi.org/10.1103/PhysRevLett.122.208101>
- Gauriau, C., & Bernard, J.-F. (2004). Posterior triangular thalamic neurons convey nociceptive messages to the secondary somatosensory and insular cortices in the rat. *Journal of Neuroscience*, *24*(3), 752–761.
- Hong, G., & Lieber, C. M. (2019). Novel electrode technologies for neural recordings. *Nature Reviews Neuroscience*, *20*(6), 330–345
- Hubel, D. H. (1957). Tungsten microelectrode for recording from single units. *Science*, *125*(3247), 549–550.
- Hubel, D. H., & Wiesel, T. N. (1959). Receptive fields of single neurones in the cat's striate cortex. *J. Physiol*, *148*(3), 574–591.
- Hubel, D. H., & Wiesel, T. N. (1962). Receptive fields, binocular interaction and functional architecture in the cat's visual cortex. *The Journal of physiology*, *160*(1), 106
- Hubel, D. H., & Wiesel, T. N. (1968). Receptive fields and functional architecture of monkey striate cortex. *J. Physiol*, *195*(1), 215–243.
- Hung, C., Kreiman, G., Poggio, T., & DiCarlo, J. (2005). Fast readout of object identity from macaque inferior temporal cortex. *Science*, *310*(5749), 863–866.
- Jun, J. J., Steinmetz, N. A., Siegle, J. H., Denman, D. J., Bauza, M., Barbarits, B., B., L., K., A., Anastassiou, C. A., Andrei, A., Aydn, Ç., Barbic, M., Blanche, T., Bonin, V., Couto, J., Dutta, B., Gratiy, S. L., Gutnisky, D. A., Häusser, M., ... Harris, T. D. (2017). Fully integrated silicon probes for high-density recording of neural activity. *Nature*, *551*(7679), 232–236. <https://doi.org/10.1038/nature24636>
- Kandel, E. R. (2013). *Principles of neural science* (5th ed.). McGraw-Hill.
- Kravitz, D. J., Saleem, K. S., Baker, C. I., & Mishkin, M. (2011). A new neural framework for visuospatial processing. *Nature Reviews Neuroscience*, *12*(4), 217–230.
- Lashley, K. S. (1930). Basic neural mechanisms in behavior. *Psychological review*, *37*(1), 1.
- LeDoux, J. E., Sakaguchi, A., & Reis, D. J. (1984). Subcortical efferent projections of the medial geniculate nucleus mediate emotional responses conditioned to acoustic stimuli. *Journal of Neuroscience*, *4*(3), 683–698
- Marshall, J. H., Garrett, M., Garrett, M. E., Nauhaus, I., & Callaway, E. M. (2011). Functional specialization of seven mouse visual cortical areas. *Neuron*, *72*(6), 1040–1054. <https://doi.org/10.1016/j.neuron.2011.12.004>
- Nicolelis, M. A., Ghazanfar, A. A., Faggin, B. M., Votaw, S., & Oliveira, L. M. (1997). Reconstructing the engram: Simultaneous, multisite, many single neuron recordings. *Neuron*, *18*(4), 529–537.
- Nicolelis, M. A., & Lebedev, M. A. (2009). Principles of neural ensemble physiology underlying the oper-

- ation of brain-machine interfaces. *Nature reviews neuroscience*, *10*(7), 530–540.
- Nicolelis, M. A. L., Dimitrov, D., Carmena, J. M., Crist, R., Lehew, G., Kralik, J. D., & Wise, S. P. (2003). Chronic, multisite, multielectrode recordings in macaque monkeys. *Proc. Natl. Acad. Sci. U. S. A*, *100*(19), 11041–11046.
- Niell, C. M., & Stryker, M. P. (2008). Highly selective receptive fields in mouse visual cortex. *Journal of Neuroscience*, *28*(30), 7520–7536.
- O'Keefe, J. (1976). Place units in the hippocampus of the freely moving rat.
- O'Mara, S. (2005). The subiculum: What it does, what it might do, and what neuroanatomy has yet to tell us. *Journal of anatomy*, *207*(3), 271–282.
- Paxinos, G., & Franklin, K. (2001). *The mouse brain in stereotaxic coordinates*. Academic press.
- Powell, T. P., & Mountcastle, V. B. (1959). Some aspects of the functional organization of the cortex of the postcentral gyrus of the monkey: A correlation of findings obtained in a single unit analysis with cytoarchitecture. *Bull. Johns Hopkins Hosp*, *105*, 133–162.
- Prusky, G., & Douglas, R. (2004). Characterization of mouse cortical spatial vision. *Vision research*, *44*(28), 3411–3418. <https://doi.org/10.1016/j.visres.2004.09.001>
- Renart, A., Rocha, J., Bartho, P., Hollender, L., Parga, N., Reyes, A., & Harris, K. D. (2010). The asynchronous state in cortical circuits. *Science*, *327*(5965), 587–590.
- Ringach, D. L. (2004). Mapping receptive fields in primary visual cortex. *The Journal of Physiology*, *558*(3), 717–728.
- Roth, M. M., Helmchen, F., & Kampa, B. M. (2012). Distinct functional properties of primary and posteromedial visual area of mouse neocortex. *The Journal of Neuroscience*, *32*(28), 9716–9726. <https://doi.org/10.1523/jneurosci.0110-12.2012>
- Smith, P. H., Manning, K. A., & Uhlrich, D. J. (2010). Evaluation of inputs to rat primary auditory cortex from the suprageniculate nucleus and extrastriate visual cortex. *Journal of Comparative Neurology*, *518*(18), 3679–3700.
- Steinmetz, N. A., Koch, C., Harris, K. D., & Carandini, M. (2018). Challenges and opportunities for large-scale electrophysiology with neuropixels probes. *Current opinion in neurobiology*, *50*, 92–100.
- Steinmetz, N. A., Aydin, C., Lebedeva, A., Okun, M., Pachitariu, M., Bauza, M., & Harris, T. D. (2021). Neuropixels 2.0: A miniaturized high-density probe for stable, long-term brain recordings. *Science*, *372*(6539), eabf4588.
- Stevenson, I. H., & Kording, K. P. (2011). February). How advances in neural recording affect data analysis. *Nat. Neurosci*, *14*(2), 139–142.
- Trautmann, E. M., Hesse, J. K., Stine, G. M., Xia, R., Zhu, S., O'Shea, D. J., Karsh, B., Colonell, J., Lanfranchi, F. F., Vyas, S., Zimnik, A., Steinmann, N. A., Wagenaar, D. A., Andrei, A., Lopez, C. M., O'Callaghan, J., Putzeys, J., Raducanu, B. C., Welkenhuysen, M., . . . Harris, T. (2023). Large-scale high-density brain-wide neural recording in nonhuman primates. *BioRxiv*. <https://doi.org/10.1101/2023.02.01.526664>
- Ungerleider, L. G., & Mishkin, M. (1982). Two cortical visual systems. In D. J. Ingle, M. A. Goodale, & R. J. W. Mansfield (Eds.), *Analysis of visual behavior* (pp. 549–586). MIT Press.
- Vasconcelos, N., Pantoja, J., Belchior, H., Caixeta, F. V., Faber, J., Freire, M. A. M., & Ribeiro, S. (2011). Cross-modal responses in the primary visual cortex encode complex objects and correlate with tactile discrimination. *Proceedings of the National Academy of Sciences*, *108*(37), 15408–15413. <https://doi.org/10.1073/pnas.1102780108>
- Wang, Q., & Burkhalter, A. (2007). Area map of mouse visual cortex. *The Journal of Comparative Neurology*, *502*(3), 339–357. <https://doi.org/10.1002/cne.21286>
- Watson, C., Paxinos, G., & Puelles, L. (2011). *The mouse nervous system*. Academic Press.
- Whitlock, J. R., Sutherland, R. J., Witter, M., Moser, M.-B., & Moser, E. (2008). Navigating from hippocampus to parietal cortex. *Proceedings of the National Academy of Sciences*, *105*(39), 14755–14762.
- Zrinzo, L., Zrinzo, L. V., & Hariz, M. (2007). The peripeduncular nucleus: A novel target for deep brain stimulation? *Neuroreport*, *18*(15), 1631–1632.

Appendix

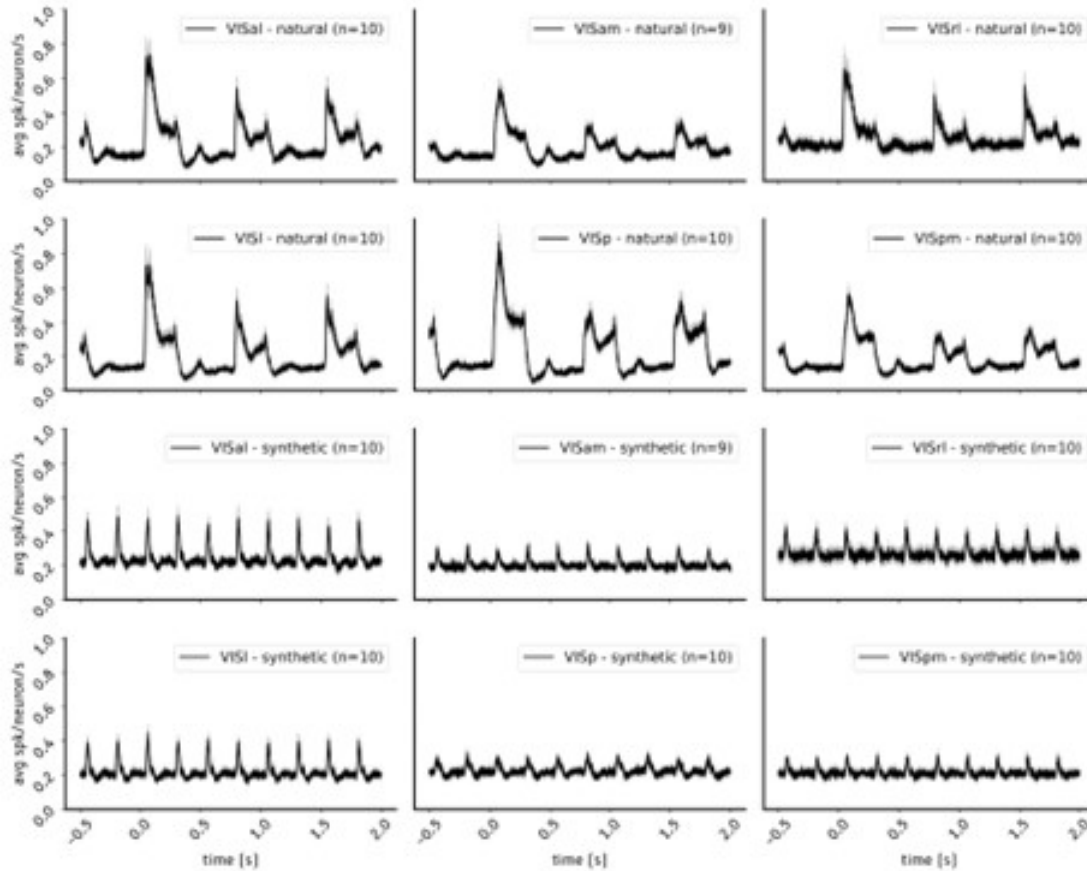
Figure 1

Exploring Spiking Activity along the Visual Cortex


Note. (VIS al = anterolateral, am = anteromedial, rl = rostrolateral, l = lateromedial, p = primary visual cortex, pm = posteromedial) (a) general overview of different periods of recordings: 60min-long of natural images rewarded exposure; 25min-long of synthetic images (Gabor); 60min-long of natural images non-rewarded exposure. (b) samples of a total of 945 identified receptive fields along the visual cortex out of 4650 units (#VISal=177, #VISam=110, #VISl=257, #VISp=173, #VISpm=143, #VISrl=85). (c) spiking correlation structures along the visual cortex ($n = 19659$), with the following averages: VISal = .0167, VISam = .0052, VISl = .0164, VISp = .0164, VISpm = .0071, VISrl = .0114.

Figure 2

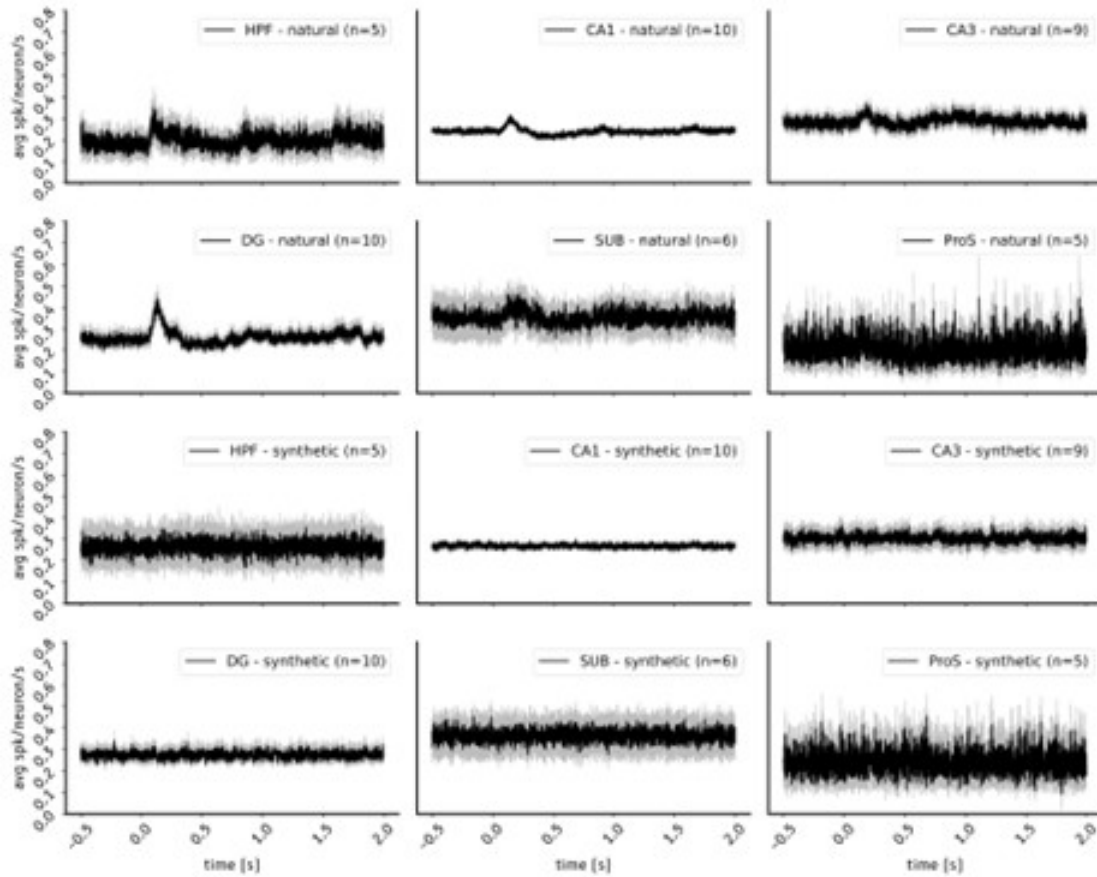
Group PSTH (peristimulus time histogram) Result in Different Regions of the Visual Cortex . (VIS al=anterolateral, am=anteromedial, rl=rostromedial, l=lateromedial, p=primary visual cortex, pm=posteromedial) for two Different Classes of Visual Stimuli



Note. (duration 2.5 s, 100 samples/session/class randomly selected): natural and synthetic (Gabor); number of sessions ($n = 10$, $n = 9$) indicated in each plot; vertical axis with mean instantaneous firing rate of the population (spikes/neuron/second).

Figure 3

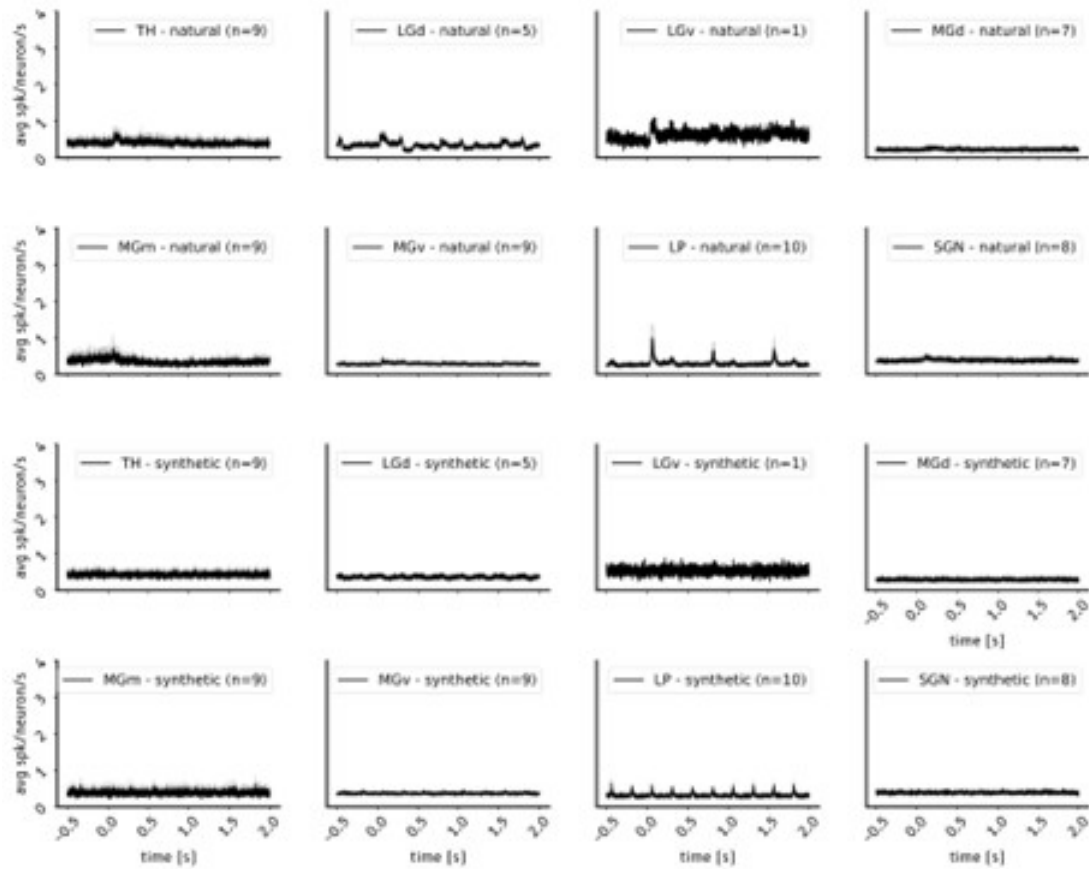
Group PSTH (peristimulus time histogram) Result in Different Regions of the Hippocampus (HPF, CA1, CA3, DG, SUB, ProS) for two Different Visual Stimulus Classes



Note. (duration 2.5 s, 100 samples/session/class randomly chosen): natural and synthetic (Gabor); number of sessions ($n = 10$, $n = 9$, $n = 6$, and $n = 5$) indicated on each plot; vertical axis with the mean instantaneous firing rate of the population (spikes/neuron/second).

Figure 4

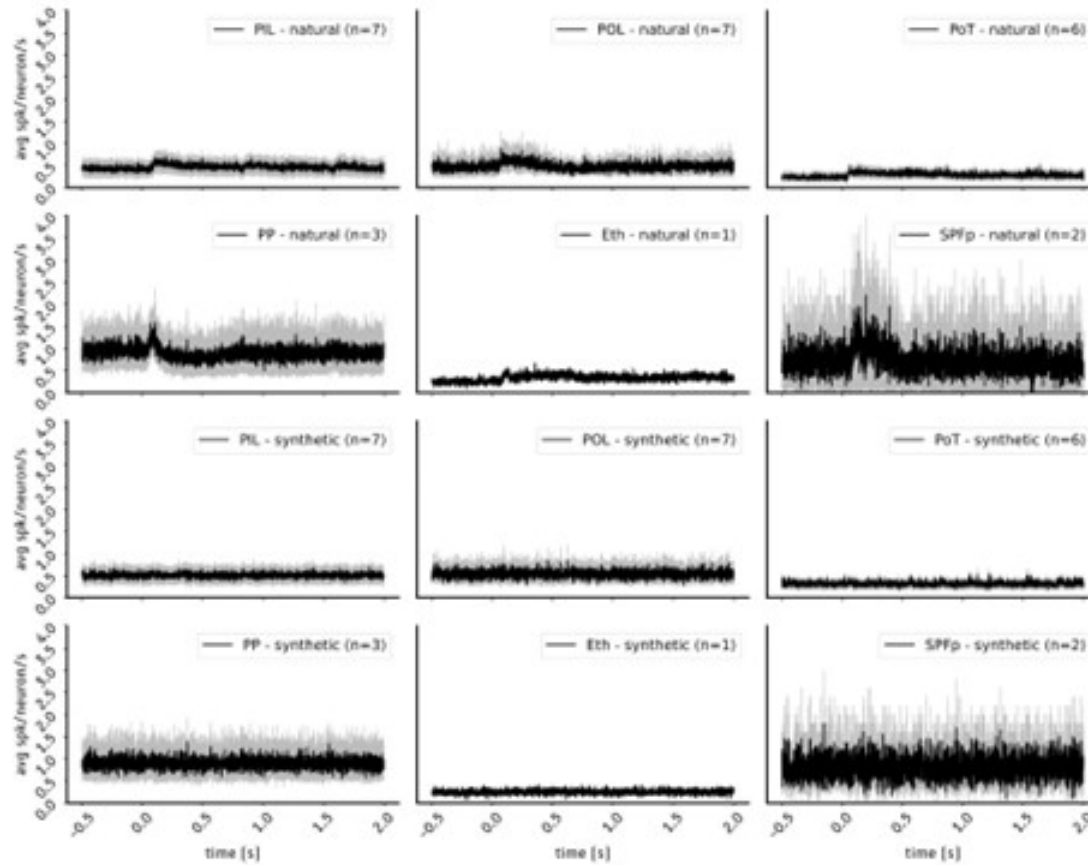
Group PSTH (peristimulus time histogram) Result in Different Regions of the Thalamus (LP, MGv, MGm, TH, SGN, MGd, LGd, LGv) for two Different Visual Stimulus Classes



Note. (duration 2.5 s, 100 samples/session/class randomly chosen): natural and synthetic (Gabor); number of sessions ($n = 10$, $n = 9$, $n = 8$, $n = 7$, $n = 5$ and $n = 1$) indicated on each plot; vertical axis with the mean instantaneous firing rate of the population (spikes/neuron/second).

Figure 5

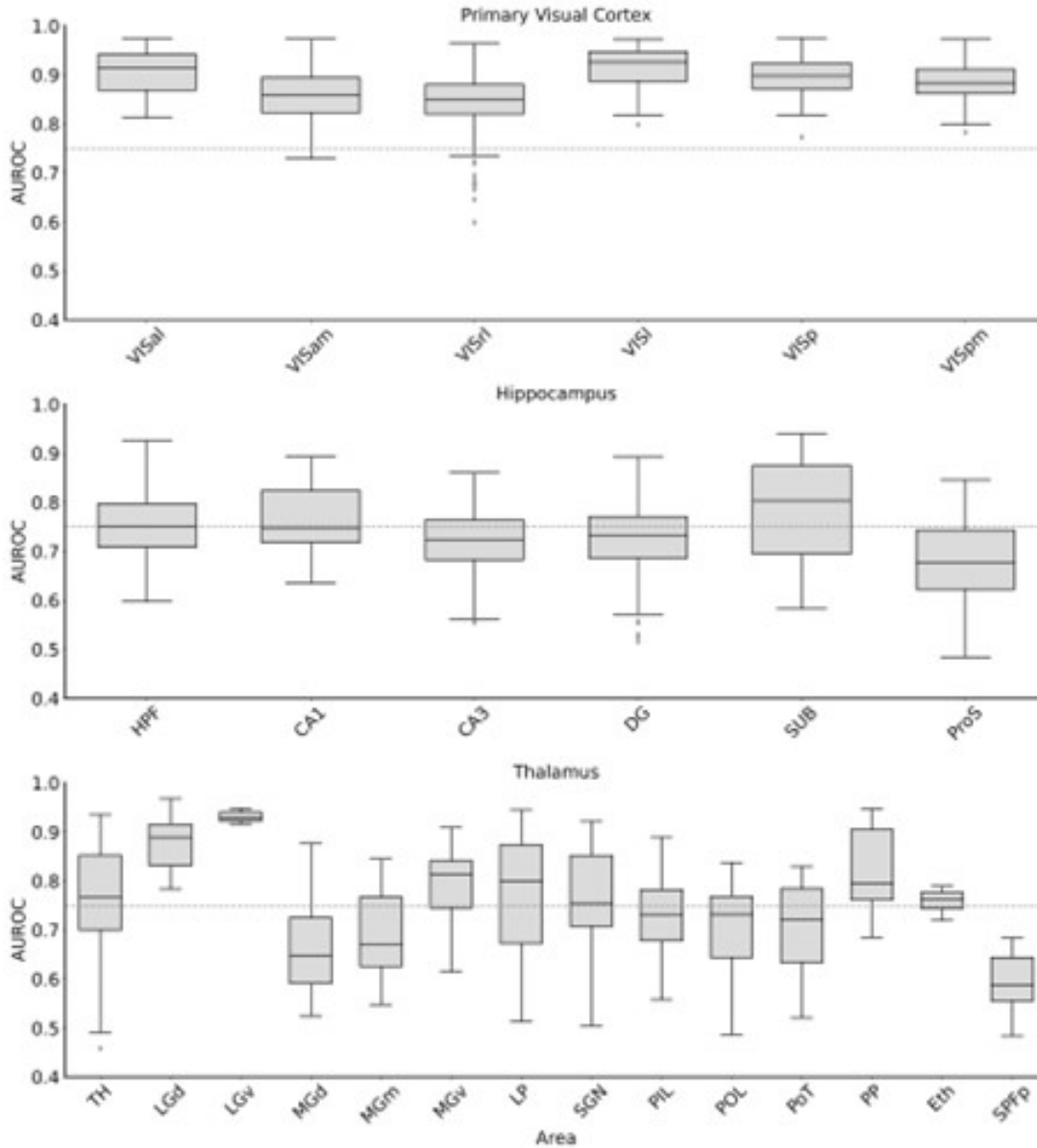
Group PSTH (peristimulus time histogram) Result in Different Regions of the Thalamus (PIL, POL, PoT, PP, Eth, SPFp) for two Different Visual Stimulus



Note. (duration 2.5 s, 100 samples/session/class randomly chosen): natural and synthetic (Gabor); number of sessions ($n = 7$, $n = 6$, $n = 3$, $n = 2$, and $n = 1$) indicated on each plot; vertical axis with the mean instantaneous firing rate of the population (spikes/neuron/second).

Figure 6

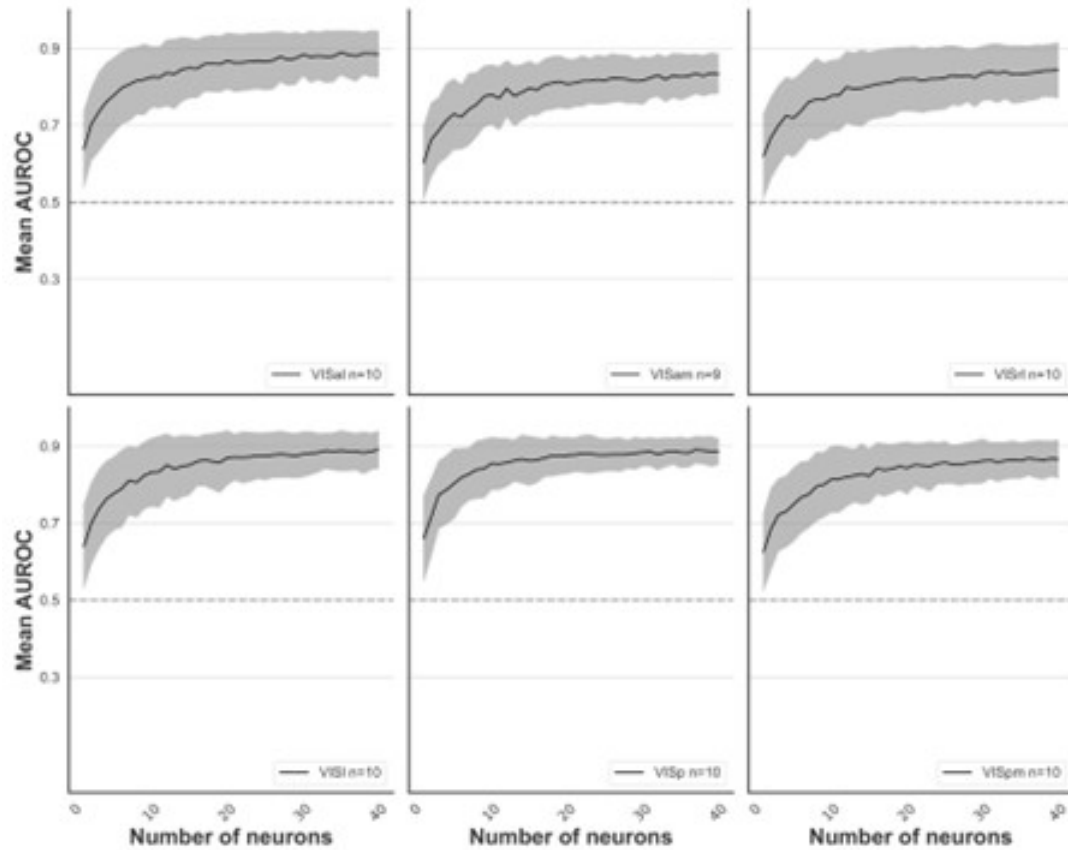
Boxplot showing the Results of Naïve Bayes Classification with the Total Available Neurons in Different Regions of the Visual Cortex



Note. (VIS al=anterolateral, am=anteromedial, rl=rostrolateral, l=lateromedial, p=primary visual cortex, pm=posteromedial), hippocampus (HPF, CA1, CA3, DG, SUB, ProS) and thalamus (TH, LGd, LGv, MGd, MGvm, MGv, LP, SGN, PIL, POL, PoT, PP, Eth, SPFP) for two different classes of visual stimuli: natural and synthetic (Gabor); using NB classifier; vertical axis represents the average value of the ROC curve area for the classification. Dotted gray line at .75 indicates the good classification quality threshold.

Figure 7

Group Result of Classification in Different Regions of the Visual Cortex



Note. (VIS al=anterolateral, am=anteromedial, rl=rostrolateral, l=lateromedial, p=primary visual cortex, pm=posteromedial) for two different visual stimulus classes: natural and synthetic (Gabor); Naive Bayes classifier; number of sessions ($n = 10$, $n = 9$) indicated in each plot; vertical axis with the average value of the ROC curve area for the classification.

Figure 8

Group result of classification in different regions of the hippocampus (HPF, CA1, CA3, DG, SUB, ProS) for two different classes of visual stimuli: natural and synthetic (Gabor); Naive Bayes classifier; number of sessions ($n = 10$, $n = 9$, $n = 6$, and $n = 5$) indicated in each plot; vertical axis with the average value of the ROC curve area for the classification.

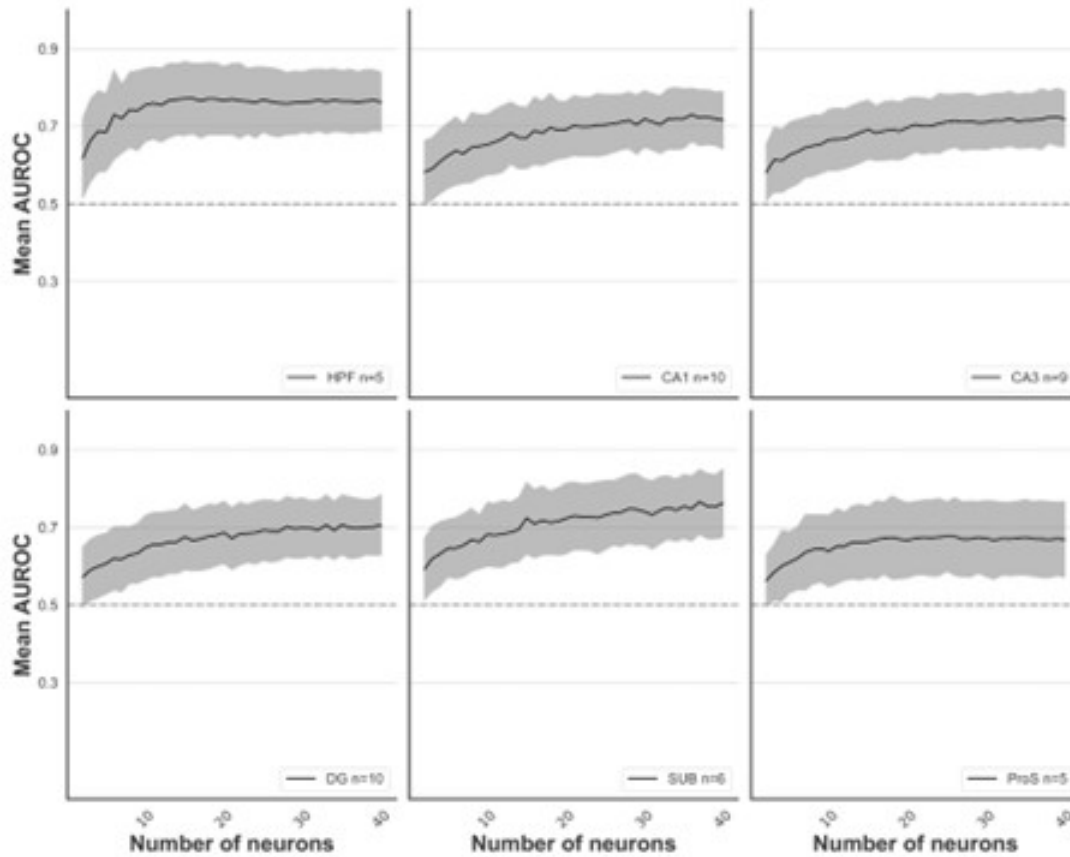
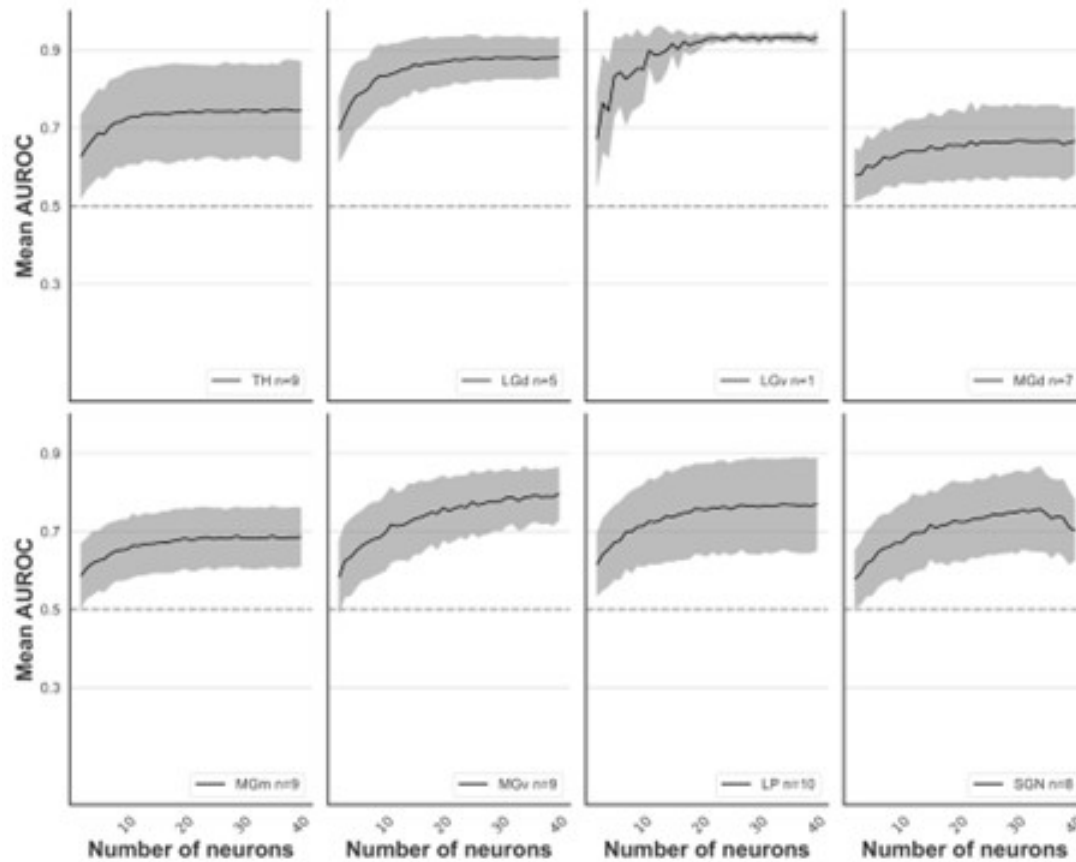


Figure 9

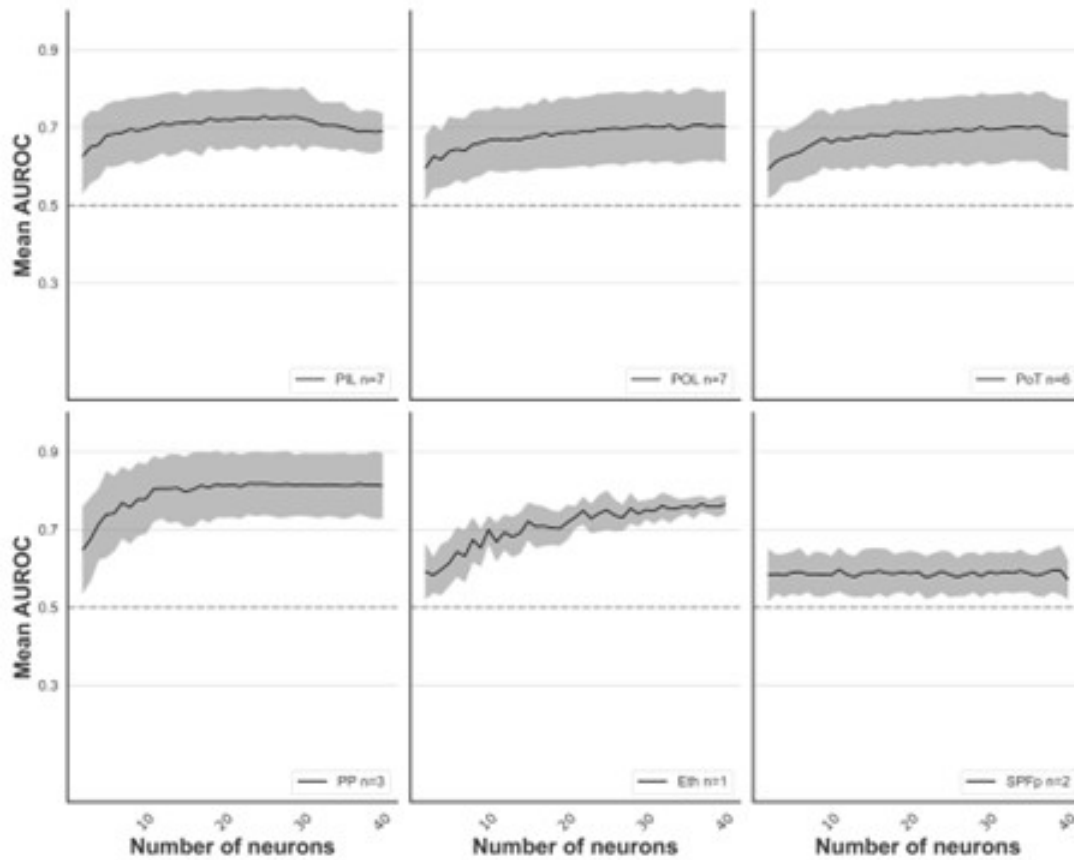
Group Result of Classification in Different Regions of the Thalamus



Note. (LP, MGv, MGm, TH, SGN, MGd, LGd, LGv) for two different classes of visual stimuli: natural and synthetic (Gabor); Naive Bayes classifier; number of sessions ($n = 10$, $n = 9$, $n = 8$, $n = 7$, $n = 5$, and $n = 1$) indicated in each plot; vertical axis with the average value of the ROC curve area for the classification.

Figure 10

Group Result of Classification in Different Regions of the Thalamus



Note. (PIL, POL, PoT, PP, SPFp, Eth) for two different classes of visual stimuli: natural and synthetic (Gabor); Naive Bayes classifier; number of sessions ($n = 6$, $n = 5$, $n = 3$, $n = 2$, and $n = 1$) indicated in each plot; vertical axis with the average value of the ROC curve area for the classification.